22nd Australasian Fluid Mechanics Conference AFMC2020
Brisbane, Australia, 7–10 December 2020
https://doi.org/10.14264/05a39db

Resolvent analysis predictions of energy transfer in turbulent channel flow

S. Symon[1], **S. J. Illingworth**[1] **and I. Marusic**[1]

[1] Department of Mechanical Engineering
University of Melbourne, Parkville VIC 3010, Australia

Abstract

We analyse the inter-scale transfer of energy for turbulent channel flow at $Re_\tau = 180$ in a minimal flow unit. The dominant energy-producing modes are streamwise-constant streaks with a spanwise spacing of approximately 100 wall units. Since the viscous dissipation for these scales is not sufficient to balance production, the nonlinear terms redistribute the excess energy to other scales. We compare the energy balance to predictions from resolvent analysis and show that it does not model energy transfer well. Nevertheless, we find that the energy transferred from the streamwise-constant streaks can be predicted reasonably well by a Cess eddy viscosity profile. As such, eddy viscosity is an effective model for the nonlinear terms in resolvent analysis and explains good predictions for the most energetic streamwise-constant streaks. Eddy viscosity does not respect the conservative nature of nonlinear transfer and is less effective for scales which receive energy from the nonlinear terms.

Keywords
turbulence; resolvent analysis; energy transfer; reduced-order modelling

Introduction

Energy transfer plays a key role in the organisation and evolution of turbulent flows. It is responsible for the multi-scale nature of turbulence and lends insight into the self-sustaining process [5]. Energy transfer for an individual scale is described by the spectral turbulent kinetic energy (TKE) equation, which contains a nonlinear term referred to as turbulent transport. Nonlinearity poses considerable theoretical difficulties by permitting inter-scale energy exchange [4]. An improved understanding of nonlinear interactions in turbulent flows, therefore, is essential to improve turbulence modelling and simulation.

It is also known that linear mechanisms are important in energy transfer. These are described well by the linear operator obtained after linearising the Navier-Stokes equations around a suitable base flow [12]. Linear mechanisms have also been identified in mean (time-averaged) flows by resolvent analysis [10]. In this framework, the equations are linearised around the mean flow to obtain the resolvent operator that maps the nonlinear terms, treated as an intrinsic forcing, to the velocity in the frequency domain.

In this study, we investigate the extent to which energy transfer is correctly modelled by resolvent analysis. To address this question, we first examine how energy is produced, dissipated, and transferred among various scales of turbulent channel flow in a "minimal flow unit" [7]. We calculate these terms in spectral space and integrate them over the wall-normal direction. The true energy transfer from direct numerical simulation (DNS) is compared to predictions from resolvent analysis. We show that the agreement can be improved by adding the Cess [2] eddy viscosity profile to the resolvent as done in many studies [6]. Eddy viscosity serves as a model for the role of nonlinear transfer in resolvent analysis and we quantify its contribution to the energy balance for each scale.

Methods

The non-dimensional Navier-Stokes equations for statistically steady, turbulent channel flow are

$$\frac{\partial \boldsymbol{u}}{\partial t} + \boldsymbol{u}\cdot\boldsymbol{\nabla}\boldsymbol{u} = -\boldsymbol{\nabla}p + \frac{1}{Re_\tau}\boldsymbol{\nabla}^2\boldsymbol{u}, \tag{1}$$

$$\boldsymbol{\nabla}\cdot\boldsymbol{u} = 0, \tag{2}$$

where $\boldsymbol{u} = [u,v,w]^T$ is the velocity in the x (streamwise), y (spanwise) and z (wall-normal) directions and p is the pressure. The friction Reynolds number $Re_\tau = u_\tau h/\nu$ is defined in terms of the friction velocity u_τ, channel half height h, and kinematic viscosity ν. No-slip boundary conditions are applied at the walls and periodic boundary conditions are imposed in the streamwise and spanwise directions. The density of the fluid is ρ and the velocities are non-dimensionalized by u_τ, the spatial variables by h and the pressure by ρu_τ^2. A '+' superscript denotes spatial variables that have been normalized by the viscous length scale ν/u_τ.

Resolvent analysis

We begin by Reynolds-decomposing equation (1), which leads to the following equations for the fluctuations:

$$\frac{\partial \boldsymbol{u}'}{\partial t} + \boldsymbol{U}\cdot\boldsymbol{\nabla}\boldsymbol{u}' + \boldsymbol{u}'\cdot\boldsymbol{\nabla}\boldsymbol{U} + \boldsymbol{\nabla}p' - \frac{1}{Re_\tau}\boldsymbol{\nabla}^2\boldsymbol{u}' = \boldsymbol{f}', \tag{3}$$

where $\bar{(\cdot)}$ and $(\cdot)'$ denote a time-average and fluctuation, respectively. The time-averaged velocity field is $\boldsymbol{U} = [U(z),0,0]^T$ and $\boldsymbol{f}' = -\boldsymbol{u}'\cdot\boldsymbol{\nabla}\boldsymbol{u}' + \overline{\boldsymbol{u}'\cdot\boldsymbol{\nabla}\boldsymbol{u}'}$ contains the nonlinear terms. Equation (3) is Fourier-transformed in time and in the homogeneous directions x and y and recast into input-output form

$$\hat{\boldsymbol{u}}(\boldsymbol{k}) = \boldsymbol{C}(i\omega\boldsymbol{I} - \boldsymbol{A})^{-1}\hat{\boldsymbol{f}}(\boldsymbol{k}) = \mathcal{H}(\boldsymbol{k})\hat{\boldsymbol{f}}(\boldsymbol{k}), \tag{4}$$

where $\hat{(\cdot)}$ denotes the Fourier-transformed coefficient, k_x is the streamwise wavenumber, k_y is the spanwise wavenumber and ω the temporal frequency. The equivalent wavelengths in the streamwise and spanwise directions are $\lambda_x = 2\pi/k_x$ and $\lambda_y = 2\pi/k_y$. The operators $\boldsymbol{A}$, $\boldsymbol{B}$ and $\boldsymbol{C}$ represent the linear Navier-Stokes operator, the input matrix and the output matrix, respectively (see [**?**] for more details). $\mathcal{H}(\boldsymbol{k})$ is a linear operator called the resolvent that relates the input forcing $\hat{\boldsymbol{f}}(\boldsymbol{k})$ to the output velocity $\hat{\boldsymbol{u}}(\boldsymbol{k})$. It depends on the wavenumber triplet $\boldsymbol{k} = (k_x, k_y, \omega)$ although this dependence is omitted in what follows for conciseness. The resolvent identifies structures amplified by linear mechanisms and they can be obtained from a singular value decomposition of $\mathcal{H}$:

$$\mathcal{H} = \hat{\boldsymbol{\Psi}}\boldsymbol{\Sigma}\hat{\boldsymbol{\Phi}}^*, \tag{5}$$

where $\hat{\boldsymbol{\Psi}} = [\hat{\boldsymbol{\psi}}_1, \hat{\boldsymbol{\psi}}_2, \cdots, \hat{\boldsymbol{\psi}}_p]$ and $\hat{\boldsymbol{\Phi}} = [\hat{\boldsymbol{\phi}}_1, \hat{\boldsymbol{\phi}}_2, \cdots, \hat{\boldsymbol{\phi}}_p]$ are orthogonal basis functions for the velocity and nonlinear forcing, respectively. The diagonal matrix $\boldsymbol{\Sigma}$ ranks the pth structure by its gain σ_p using an inner product that is proportional to its kinetic energy.

Energy balance

We now derive the energy balance that must be satisfied by the velocity field and individual resolvent modes. Equation (3) is rewritten in index notation

$$\frac{\partial u_i'}{\partial t} + U_j \frac{\partial u_i'}{\partial x_j} + u_j' \frac{\partial U_i}{\partial x_j} + \frac{\partial p'}{\partial x_i} - \frac{1}{Re}\frac{\partial^2 u_i'}{\partial x_j \partial x_j} = -f_i'. \quad (6)$$

The indices $i, j = 1,2,3$ and it can be noted that $U_1 = U, U_j = 0$ if $j = 2,3$ and $\partial U_i/\partial x_j \neq 0$ for $i = 1$ and $j = 3$ only. The kinetic energy for a specific spatial scale is obtained after multiplying equation (6) by $u_i'^*$ and Fourier-transforming in x and y. The result is integrated over z and time-averaged to arrive at the spectral turbulent kinetic energy (TKE) equation:

$$\underbrace{-\int_{-h}^{h} \frac{dU}{dz}\overline{\hat{u}^*\hat{w}}dz}_{\hat{P}(k_x,k_y)} \underbrace{-\frac{1}{Re}\int_{-h}^{h}\overline{\frac{\partial \hat{u}_i}{\partial x_j}\frac{\partial \hat{u}_i^*}{\partial x_j}}dz}_{\hat{D}(k_x,k_y)} \underbrace{-\int_{-h}^{h}\overline{\hat{u}_i^*\frac{\partial}{\partial x_j}\widehat{u_i u_j}}dz}_{\hat{N}(k_x,k_y)} = 0. \quad (7)$$

The pressure terms vanish after integrating over the full channel. We consider the real part of equation (7), which consists of three terms: production, viscous dissipation and nonlinear transfer. In general, production $\hat{P}$ is positive for a given scale as perturbations extract energy from the mean flow. Viscous dissipation $\hat{D}$, on the other hand, is guaranteed to be real and negative as it is the mechanism through which kinetic energy is removed from the system and converted into heat. Nonlinear transfer $\hat{N}$ may be positive or negative depending on the scale selected. If $\hat{P} > \hat{D}$, for example, then $\hat{N} < 0$ in order to achieve a balance. In a similar fashion, if $\hat{P} < \hat{D}$, then $\hat{N} > 0$. The integral of $\hat{N}$ over all k_x and k_y, nevertheless, is zero.

To obtain the energy balance for resolvent modes, equation (6) is multiplied by $u_i'^*$ and Fourier-transformed in x, y and t. The result is integrated over the wall-normal direction to obtain

$$\int_{-h}^{h}\frac{dU}{dz}\hat{u}^*\hat{w}dz - \frac{1}{Re}\int_{-h}^{h}\frac{\partial \hat{u}_i}{\partial x_j}\frac{\partial \hat{u}_i^*}{\partial x_j}dz - \int_{-h}^{h}\hat{u}_i^*\hat{f}_i dz = 0. \quad (8)$$

In this form, the nonlinear forcing $\hat{\boldsymbol{f}}$ appears explicitly in the energy balance. Assuming $\hat{\boldsymbol{f}}$ is white noise, the velocity field can be expressed in terms of resolvent modes

$$\hat{\boldsymbol{u}} = \sum_{p=1}^{N}\hat{\boldsymbol{\Psi}}_p\sigma_p. \quad (9)$$

Substituting equation (9) into equation (8) yields

$$\sum_p \sigma_p\left(\int_{-h}^{h}\frac{dU}{dz}\hat{\boldsymbol{\Psi}}_p^{*,i=1}\hat{\boldsymbol{\Psi}}_p^{j=3}dz + \frac{1}{Re}\int_{-h}^{h}\frac{\partial \hat{\boldsymbol{\Psi}}_p^{*,i}}{\partial \boldsymbol{x}_j}\frac{\partial \hat{\boldsymbol{\Psi}}_p^{i}}{\partial \boldsymbol{x}_j}dz\right) + \sum_p\int_{-h}^{h}\boldsymbol{\Psi}_p^*\hat{\boldsymbol{\Phi}}_p dz = 0. \quad (10)$$

Each term in the sum can be decoupled since the basis functions $\hat{\boldsymbol{\Psi}}_p$ are orthogonal. This means that production, dissipation and nonlinear transfer must be balanced across each resolvent mode. For simplicity, this study focuses on the optimal resolvent mode only, i.e. $p = 1$.

Eddy viscosity model

Instead of treating $\hat{\boldsymbol{f}}$ as white noise, its effect can be modelled by adding the Cess eddy viscosity profile [2] to the linearised equations [11, 6]

$$\nu_T(z) = \frac{\nu}{2}\left(1 + \left[\frac{\kappa}{3}(1-z^2)(1+2z^2)\left(1 - e^{|z-1|\frac{Re_\tau}{A}}\right)\right]^2\right)^{1/2} + \frac{\nu}{2}, \quad (11)$$

where $\kappa = 0.426$ and $A = 25.4$ are chosen based on a least-squares fit to experimentally obtained mean velocity profiles at $Re_\tau = 2000$ [1]. The eddy viscosity introduces two terms into the energy balance

$$\widehat{Edd}(k_x,k_y) = \underbrace{-\int_{-h}^{h}(\nu_T(z)-\nu)\overline{\frac{\partial \hat{u}_i}{\partial x_j}\frac{\partial \hat{u}_i^*}{\partial x_j}}dz}_{\hat{V}(k_x,k_y)} \underbrace{-\int_{-h}^{h}\frac{d\nu_T}{dz}\overline{\left(\hat{u}_i^*\frac{\partial \hat{u}_i}{\partial y} + \hat{u}_i^*\frac{\partial \hat{w}}{\partial x_i}\right)}dz}_{\hat{G}(k_x,k_y)}, \quad (12)$$

where the kinematic viscosity ν has been subtracted in order to remove the contribution of viscous dissipation $\hat{D}(k_x,k_y)$. The remainder $\hat{V}(k_x,k_y)$ represents additional dissipation provided by the wall-normal varying portion of ν_T. The second term $\hat{G}(k_x,k_y)$ is related to the wall-normal gradient of ν_T. The combined effect of $\hat{V}(k_x,k_y)$ and $\hat{G}(k_x,k_y)$ is referred to as eddy dissipation $\widehat{Edd}(k_x,k_y)$. The metric

$$\varepsilon(k_x,k_y) = \frac{\widehat{Edd}(k_x,k_y) - \hat{N}(k_x,k_y)}{|\hat{N}(k_x,k_y)|}, \quad (13)$$

is the accuracy of the eddy viscosity in modelling $\hat{N}(k_x,k_y)$ for a given scale.

Flow description

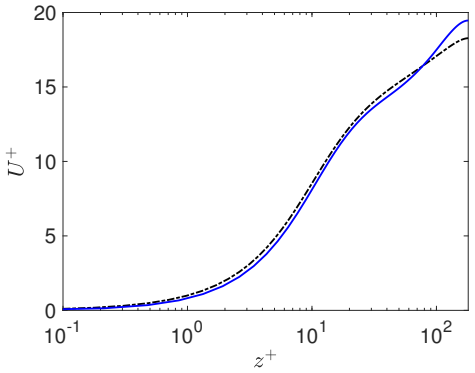

Figure 1. Mean velocity profiles for the minimal channel (blue) and the DNS of [8] (black).

The minimal channel flow is computed for $Re_\tau = 180$ using an unstructured finite difference solver (see [3] for details) on a domain with dimensions $\pi \times \pi/4 \times 2h$ in the streamwise, spanwise and wall-normal directions. There are 96 and 48 equally spaced points in the streamwise and spanwise directions, respectively, and 128 points in the wall-normal direction on a Chebyshev grid. The minimal channel mean profile is in good agreement with the mean profile of [8] for most areas of the flow other than the wake region, where the minimal channel mean profile overshoots the one from [8]. This phenomenon stems from the fact that the minimal domain is too small to accommodate the largest structures which reside in the outer region. Despite this disagreement, there is no impact on near-wall turbulence in the buffer and viscous regions where the bulk of energy resides [7].

Results

The kinetic energy is computed for the most energetic wavenumber pairs

$$\hat{E}(k_x,k_y) = \frac{1}{2}\left(\overline{\hat{u}^2(k_x,k_y) + \hat{v}^2(k_x,k_y) + \hat{w}^2(k_x,k_y)}\right), \quad (14)$$

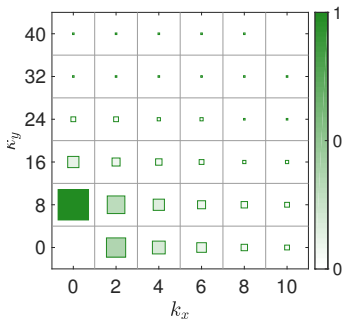

Figure 2. The kinetic energy $\hat{E}(k_x,k_y)$ of the most energetic wavenumber pairs in the minimal channel. The area and colour intensity of the square marker at the centre of each tile are directly proportional to the kinetic energy.

and plotted in figure 2. The area and colour intensity of the square marker at the centre of each tile are directly proportional to the kinetic energy. The most energetic scale is streamwise-constant with a spanwise width of approximately 100 wall units. Most of the kinetic energy, futhermore, is concentrated in structures with small streamwise and spanwise wavenumbers. To facilitate visualisation later in the paper, we choose to plot only those wavenumber pairs that appear in figure 2 although the energy balance will be computed across all of them.

DNS energy balance

Production, dissipation and nonlinear transfer for the minimal channel are illustrated in figure 3. For almost all wavenumber pairs shown, production is positive as seen in figure 3(a) with the maximum occurring for $(k_x,k_y) = (0,8)$ - this will be referred to as $(0,8)$ for brevity. The only scales where production is negative are spanwise-constant, i.e. $k_y = 0$. The dissipation in figure 3(b) is negative for all scales, as expected. Unlike production in figure 3(a), however, there is no dominant scale which is primarily responsible for dissipating energy. In fact, it can be observed that dissipation is significantly lower than production for $(0,8)$, necessitating inter-scale energy transfer to achieve an overall balance.

The nonlinear transfer in figure 3(c) illustrates that the surfeit of energy not dissipated by viscosity from $(0,8)$ is redistributed to other scales. In other words, since $\hat{P} > \hat{D}$, nonlinear transfer removes energy from $(0,8)$, i.e. $\hat{N} < 0$. It can be noted that all scales which lose energy due to nonlinear transfer are clustered around low streamwise and spanwise wavenumbers. This is consistent with the turbulence cascade in that energy from the large-scales trickles down to smaller scales which are more effective at dissipating energy.

For the majority of scales, $\hat{P} < \hat{D}$. In order to achieve a balance, therefore, they receive energy from nonlinear transfer, i.e. $\hat{N} > 0$. The largest recipients of energy through nonlinear transfer are spanwise-constant structures. This is consistent with the fact that production for these scales is either small or negative. Therefore, high nonlinear transfer is needed to counterbalance both production and dissipation. The phenomenon of energy transfer from low streamwise, high spanwise wavenumbers to high streamwise, low spanwise wavenumbers can be interpreted as a transverse cascade which has been observed in other flows such as homogeneous shear turbulence [9].

Resolvent energy balance

We compare the DNS energy balance in figure 3 to predictions from the first resolvent mode in figure 4. Since each wavenumber pair has a distribution of energetic temporal frequencies, it is necessary to choose a particular ω. To do so, we compute the singular values across a discretisation of ω and choose the ω that results in the largest amplification. As one example, $\omega = 0$ leads to the largest amplification for $(0,8)$. The resolvent results for production are plotted in figure 4(a) and they are similar to the true values in figure 3(a). The most notable difference is that the resolvent production predicted for $(0,8)$ is slightly larger with respect to the other scales. In fact, it is so dominant that production for scales such as $(0,40)$ appear as zero.

The results for viscous dissipation are illustrated in figure 4(b). Unlike the DNS case, the resolvent-predicted dissipation is sufficient to completely counteract production for the majority of scales considered. Since the sum of all three terms must be zero for each resolvent mode, it follows that nonlinear transfer is negligible for nearly all scales as seen in figure 4(c). Thus it can be concluded that resolvent analysis can identify the scales responsible for the bulk of production in the flow. It does not, however, provide good predictions for nonlinear transfer.

To identify for which scales eddy viscosity can model nonlinear transfer, the eddy dissipation is computed and displayed in figure 5(a). As expected, it is negative for all scales even though nonlinear transfer tends to be positive outside the cluster around $(0,8)$. The error ε, as defined in equation (13), is thus large for the majority of scales as seen in figure 5(b). The only scale where $\varepsilon < 1$ is $(0,8)$. Although $\varepsilon > 1$ for every other scale, those where nonlinear transfer is negative such as $(0,16)$ or $(2,8)$ have lower values of ε than scales where nonlinear transfer is positive. It can be concluded that eddy viscosity is most appropriate for the energy-producing scales whose excess energy needs to be offset by additional dissipation. Eddy viscosity, at least in its current form, is less appropriate for the scales which receive energy from nonlinear transfer.

Conclusions

We have investigated energy transfer for low Reynolds number turbulent flow in a minimal channel. Production for the energetic scales is generally positive and the largest contribution is generated by the near-wall streaks with a spanwise spacing of $\lambda_y^+ \approx 100$. Dissipation is negative for every scale although it is not sufficiently large to counteract production produced by the most energetic structures. As a result, nonlinear transfer redistributes energy to other scales such that the net effect of nonlinear transfer across all scales is zero. Spanwise-constant structures are among the largest recipients of energy through nonlinear transfer. Energy transfer in the DNS was compared to predictions from the first resolvent mode, which also has to satisfy a balance across production, dissipation and nonlinear transfer. The first resolvent mode was successful in identifying the main production mechanisms in the flow although it predicted nearly zero nonlinear transfer for every scale. Nonlinear transfer was modelled by the addition of eddy viscosity, although its quantitative accuracy was limited to the most energetic mode. Refining eddy viscosity models in the future could lead to better models for less energetic scales in the flow.

Acknowledgements

The authors acknowledge the financial support of the Australian Research Council and M. Xie for providing the DNS data.

References

[1] del Álamo, J. C. and Jiménez, J. (2006). Linear energy amplification in turbulent channels, *J. Fluid Mech.*, 559,

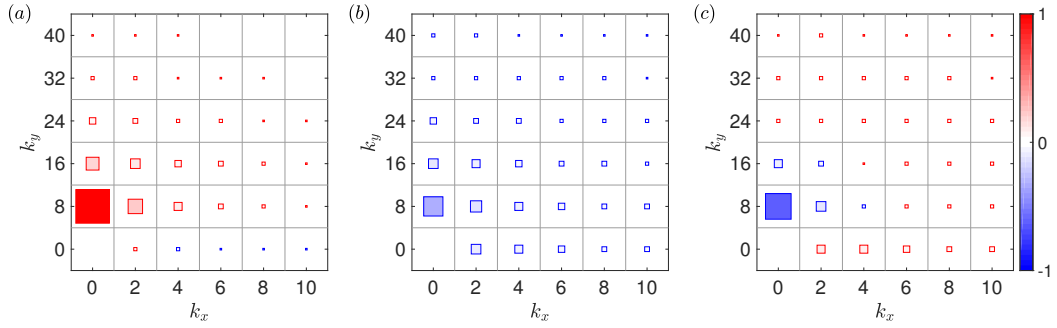

Figure 3. Contributions of (a) production, (b) dissipation and (c) nonlinear transfer to the energy balance of each Fourier mode for the minimal channel.

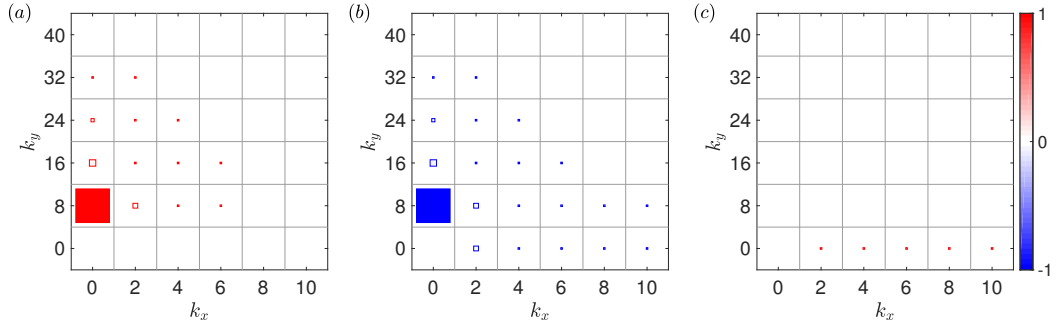

Figure 4. Contributions of (a) production, (b) dissipation and (c) nonlinear transfer from the first resolvent mode in the case of the minimal channel.

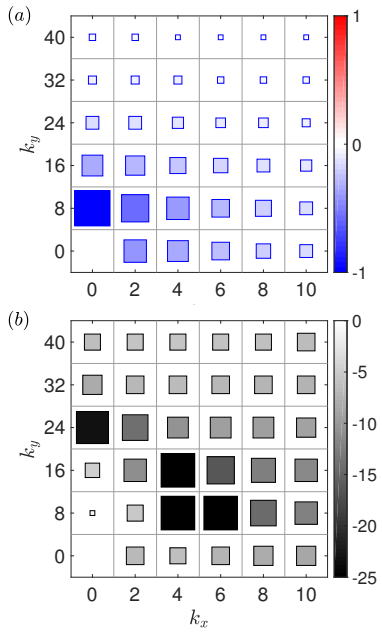

Figure 5. (a) Nonlinear transfer modelled by eddy viscosity for the minimal channel and (b) its error compared to the true nonlinear transfer in figure 3(c).

205–213.

[2] Cess, R. D. (1958). A survey of the literature on heat transfer in turbulent tube flow, Technical Report 8-0529-R24, Westinghouse Research.

[3] Chung, D., Monty, J. P. and Ooi, A. (2014). An idealised assessment of Townsend's outer-layer similarity hypothesis for wall turbulence, *J. Fluid Mech.*, 742, R3.

[4] Domaradzki, J. A., Liu, W., Härtel, C. and Kleiser, L. (1994). Energy transfer in numerically simulated wall-bounded turbulent flows, *Phys. Fluids*, 6, 1583–1599.

[5] Hamilton, J. M., Kim, J. and Waleffe, F. (1995). Regeneration mechanisms of near-wall turbulence structures, *J. Fluid Mech.*, 287, 317–348.

[6] Hwang, Y. and Cossu, C. (2010). Linear non-normal energy amplification of harmonic and stochastic forcing in the turbulent channel flow, *J. Fluid Mech.*, 664, 51–73.

[7] Jiménez, J. and Moin, P. (1991). The minimal flow unit in near-wall turbulence, *J. Fluid Mech.*, 225, 213–240.

[8] Lee, M. and Moser, R. D. (2015). Direct numerical simulation of turbulent channel flow up to $Re_\tau \approx 5200$, *J. Fluid Mech.*, 774, 395–415.

[9] Mamatsashvili, G., Khujadze, G., Chagelishvili, G., Dong, S., Jiménez, J. and Foysi, H. (2016). Dynamics of homogeneous shear turbulence: A key role of the nonlinear transverse cascade in the bypass concept, *Phys. Rev. E*, 94, 023111.

[10] McKeon, B. J. and Sharma, A. S. (2010). A critical-layer framework for turbulent pipe flow, *J. Fluid Mech.*, 658, 336–382.

[11] Reynolds, W. C. and Hussain, A. K. M. F. (1972). The mechanics of an organized shear wave in turbulent shear flow. Part 3. Theoretical models and comparisons with experiments, *J. Fluid Mech.*, 54, 263–288.

[12] Schmid, P. J. and Henningson, D. S. (2001). *Stability and transition in shear flows*, Springer.

[13] Symon, S., Illingworth, S. J. and Marusic, I. (2020). Energy transfer in turbulent channel flows and implications for resolvent modelling, *arXiv preprint arXiv:2004.13266*.